

Weighted CTDI Equation for 3D Rotational Angiography: A Monte Carlo Study

A. Azzi*, R. Hidayat, A. Rosa, L. E. Lubis

¹Departement of Physics, Faculty of Mathematics and Natural Sciences, Universitas Indonesia, Depok 16424, Indonesia

ARTICLE INFO

Article history:

Received 17 February 2023

Received in revised form 23 December 2023

Accepted 6 January 2024

Keywords:

3D rotational angiography

CTDI

Monte Carlo

CBCT

ABSTRACT

This study aims to verify the weighted Computed Tomography Dose Index (CTDI_w) coefficients of 3D rotational angiography (3DRA) procedure using Monte Carlo simulation. The Monte Carlo simulation EGSnrc usercode was employed for 3D dose simulations of the rotational angiography procedure. A virtual phantom resembles the head CTDI phantom was constructed, with a diameter of 15 cm and a density resembling polymethyl methacrylate (1.13 g/cm³). A series of virtual phantoms consisting of 5 images with ionization chamber detectors at the center position, 12 o'clock, 9 o'clock, 6 o'clock, and 3 o'clock were acquired. Simulations were performed with photon sources of 70 and 109 kVp for 200-degree x-ray tube rotation. The field of view was divided into narrow, wide, and full beam with diameters of 1.7 cm; 4.9 cm; and 8.6 cm, respectively. The simulated doses at the ionization chamber were processed into weighting factor for weighted CTDI and compared with direct measurements. The dose ratio between peripheral and center positions for 360° CBCT and 200° 3DRA was 1:1 and 1:3 in this study. The weighting factors for 3DRA were determined as CTDI_{center} = ¼ and CTDI_{periphery} = ¾. The measured average percentage difference of CTDI_w between our weighted factor and conventional CTDI_w was 1.75 % (-3.99 % to 6.08 %). The x-ray tube position of 3DRA impacted the accuracy of weighting factor of CTDI_w, with implications for the proposed weighting factor (W_{center} = ¼ and W_{periphery} = ¾) when using a 3DRA machine.

© 2024 Atom Indonesia. All rights reserved

INTRODUCTION

Angiography is the gold standard of vascular imaging during interventional radiology, interventional cardiology, or invasive surgery. Recent advancements in rotational irradiation allows this modality to generate three-dimensional (3D) images known as 3D rotational angiography (3DRA). However, one of the main concerns in 3DRA is the medical radiation dose to patients. Mostly, the dose in angiography is assessed based on Dose Air Product (DAP) and effective doses [1]. Nonetheless, DAP based evaluation is not relevant to rotational procedure. The closest method to 3DRA is tomographic procedures like Computed Tomography (CT) scan. The fundamental dose descriptor for this procedure is the CT Dose Index (CTDI₁₀₀), which involves using a 100 mm long cylindrical ionization chamber and a cylindrical phantom for measurement. As a body representative,

CTDI was measured at 5 points (1 central position and 4 peripheral positions), then weighted the results to obtain the average cross-sectional dose distribution called weighted CTDI (CTDI_w). The conventional CTDI_w for a CT scan is defined by using Eq. (1).

$$CTDI_w = \frac{1}{3}(CTDI_{100})_{center} + \frac{2}{3}(CTDI_{100})_{periphery} \quad (1)$$

However, the values 1/3 and 2/3 serve as weighted coefficients to predict the average dose across all phantoms [2], and these coefficients are designed for fan beam computed tomography (FBCT) with full (360°) x-ray tube rotation.

The 3DRA irradiation employs cone beam computed tomography (CBCT) with a rotation of less than 360° [3]. These parameters have made conventional CTDI_w unable to describe dose distribution in 3DRA. To accommodate CTDI measurements for CBCT, a previous study has advised using a point chamber in the middle of the beam [4] or pencil chamber with a length of 250 mm to cover all the secondary x-rays [5].

*Corresponding author.

E-mail address: akbar.azzi@sci.ui.ac.id

DOI:

54 However, most diagnostic radiology centers do not 109 regions: x-ray tube (BEAMnrc) and CTDI head
 55 have access to point or 250 mm long pencil 110 phantom (DOSXYZnrc). The components of the
 56 chambers to follow this recommendation. 111 x-ray tube consisted of photon source and beam
 57 Consequently, the International Atomic Energy 112 collimator. The x-ray source was defined using an
 58 Agency (IAEA) published a protocol for using a 113 x-ray spectrum generator based on a tungsten anode
 59 100 mm pencil chamber detector on a CBCT 114 spectral model using interpolating polynomials
 60 and a 32 cm diameter of the acrylic phantom. 115 (TASMIP) method with a tungsten target density of
 61 This protocol adds the ratio of the full beam width 116 8.96 g/cm^3 [16]. The spectrum results for each
 62 to the narrow plane beam width as close as 20 mm 117 energy were then converted into *spectrum* format,
 63 to the CTDI_{100} formula [6]. Furthermore, there 118 which is readable for EGSnrc. In the source
 64 was a difference of CTDI_w up to 10 % for a 200° 119 parameter, *source 1* (parallel rectangles of point
 65 and 18 % for a 180° rotation using the conventional 120 sources) was chosen, with an energy limit for
 66 equation [7,8]. 121 photons and electrons set at 10 keV, excluding the
 67 rest of the mass energy. 122

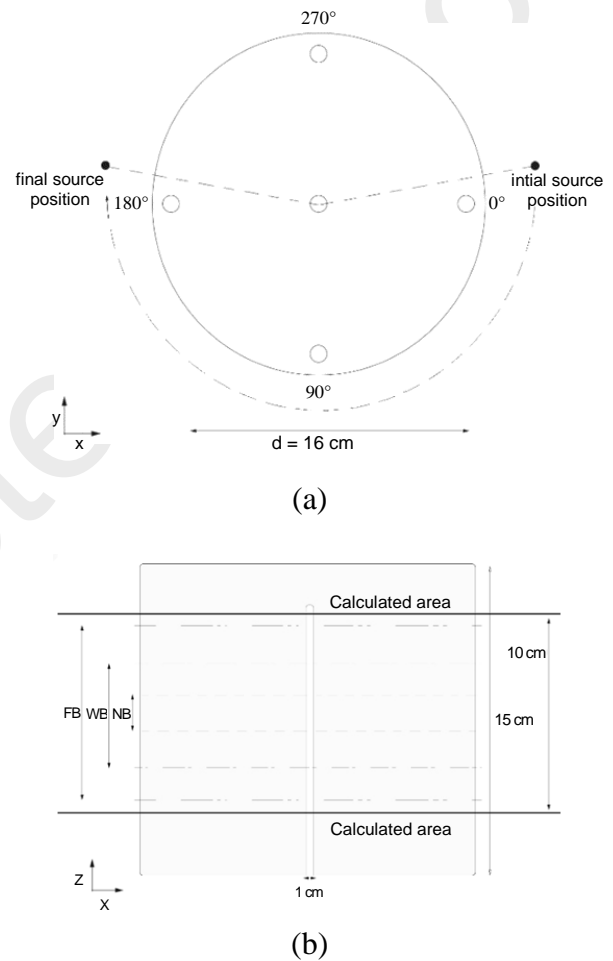
67 In addition to measurements using detectors, 123
 68 several dose calculations regarding dose distribution 124
 69 in CT have also been developed, such as CT-Expo 125
 70 (G. Stamm, Hannover, and H.D. Nagel, Buchholz, 126
 71 Germany) [9] and Virtual Dose (NIBIB, USA) [10]. 127
 72 Evaluations of these software programs indicate that
 73 tube voltage parameters influence dose distribution,
 74 but other parameters such as beam collimation or
 75 radiation width do not significantly affect changes in
 76 CT dose distribution [11]. However, several studies
 77 have reported that another type of radiation width, as
 78 well as phantom geometries, impacts the weighted
 79 coefficients. Kim, Song et al. (2011) obtained the
 80 weighted coefficients with a ratio of 50:50 for the
 81 center and periphery of the phantom for $> 40 \text{ mm}$
 82 irradiation width [12]. In addition, the Monte Carlo
 83 studies also proved that the weighted coefficients
 84 would change with the change of phantom
 85 geometries. The large range of diameter of the
 86 cylindrical phantoms reported that the weighting
 87 coefficient is more accurate with values of $3/8$ and
 88 $5/8$ for the center and periphery points than the
 89 conventional CTDI_w [13]. As for the elliptical
 90 phantom, the weighting values vary linearly
 91 following the ratio of the major and minor phantom
 92 diameters [14]. In 2021, a Monte Carlo simulation
 93 method was also be used to predict weighted CTDI
 94 for CBCT and the optimum position of ion chamber
 95 measurement points [15]. 128
 96 129

96 This study aims to determine appropriate 130
 97 CTDI_w weighted coefficient by utilizing the EGSnrc 131
 98 Monte Carlo code for a partial rotation on 3DRA 132
 99 C-arm machine and to compare the proposed 133
 100 coefficient with the conventional CTDI_w equation. 134
 101 135
 102 136
 103 137

103 METHODOLOGY

104 Monte Carlo of 3DRA

105 The Monte Carlo simulation modeled the 143
 106 delivered beam of 3DRA irradiation on the Siemens 144
 107 Artis Zee using two energy spectra i.e., 70 keV and 145
 108 109 keV. The simulation was divided into two 146

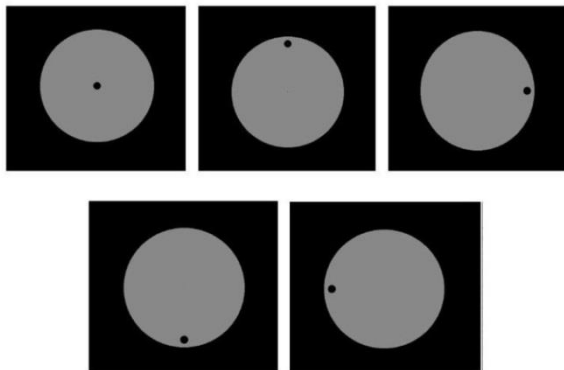


137 **Fig 1.** (a) Transversal plane of Virtual CTDI head phantom. 138
 139 A small circle inside the phantom showed an ion chamber 140
 141 positions of CTDI measurement. 0-degree position was at 142
 143 the 3 o'clock and X-ray tube rotated from 350° to 190° 144
 145 with clockwise direction (dash line). (b) Frontal plane view 146
 147 of CTDI phantom. Small cylinder at the center defined an 148
 149 example of air cavity as active volume. The algorithm 150
 151 calculated absorbed dose inside the air cavity within 152
 153 calculated area. NB, WB, and FB represented field width of 154
 155 narrow beam, wide beam, and full beam scan, respectively 156

143 The lead collimator was used to shape the 144
 145 beam width. In this research, the CTDI phantom was 146
 147 irradiated with width of 1.7 cm, 4.9 cm, and 8.6 cm 148
 149 at the midpoint of the rotation. 1.7 cm was used to 150

147 accommodate for standard fan-beam CTDI
 148 measurement. The simulation results are stored in
 149 .phps format at the lower end of the collimator
 150 component. The second region was the Monte Carlo
 151 simulation in the CTDI head phantom using
 152 DOSXYZnrc usercode. The Siemens Artis Zee
 153 3DRA machine's x-ray tube rotates by 200 degrees
 154 (from 80° to 280°), partially rotating under the
 155 phantom. For the source parameter, we selected
 156 source 8 (phase space source from multiple
 157 direction) with multiangle irradiation features.
 158 The angle of simulation indicated the position of the
 159 x-ray tube at the time the radiation is delivered.
 160 Due to the difference in polar coordinate between
 161 the phantom geometry and DOSXYZnrc baseline,
 162 there was a 90° shift in the angular position.
 163 The initial position of phase space file was placed
 164 at 350° and ended at 190°. 500 million particle
 165 histories were used for each region, energy, and
 166 beam width in the Monte Carlo simulation.
 167 Figures 1a and 1b summarize the rotational position
 168 of the x-ray tube and the width of the irradiation
 169 beam in this study.

170 Five virtual phantoms were created for a
 171 diameter resembling CTDI head phantom following
 172 the design shown in Figure 1. The virtual phantom
 173 was constructed using MATLAB version 2021a
 174 (MathWorks, Natick, Massachusetts) with a
 175 homogeneous PMMA with a density of 1.13 g/cm³
 176 and voxel dimensions of 0.1 × 0.1 × 0.1 cm³.
 177 The phantom had a diameter of 16 cm and a length of
 178 15 cm. An air cavity with diameter of 1 cm and length
 179 of 13 cm was placed at each CTDI measurement
 180 point, as shown in the axial plane of the phantom (see
 181 Fig. 2). The design of the air cavity was aimed to
 182 ensure that the Monte Carlo simulation closely
 183 resembled the measurement situation in an ion
 184 chamber, reducing systematic errors related to the
 185 mass-energy absorption ratio of medium and air.
 186 Subsequently, the virtual CTDI Phantom was
 187 converted into .egsphant format using ct-create user
 188 code.



192 Fig 2. Transversal view of virtual phantom for center, 12, 3, 6,
 193 and 9 o'clock air cavity. Point doses were obtained by
 194 calculating energy deposition inside the cavity.

195 Relative dose calculation

196 The dose calculation in this simulation was
 197 conducted on the ion chamber's active volume.
 198 Numerically, the CTDI equation in this study can be
 199 expressed as follows in Eq. (2).

$$201 \text{CTDI}_{100} = \frac{1}{N} \sum_z \sum_r \sum_\theta D_p(r \sin\theta, r \cos\theta, z) \quad (2)$$

202 where CTDI_{100} and D_p represent CTDI in Monte
 203 Carlo simulation and dose point voxel inside the air
 204 cavity, respectively. N is the irradiation field
 205 width, including narrow, wide, and full beams.
 206 The simulated x-ray tube position (θ) ranges
 207 from 0.1 to 360 degree in discrete steps.
 208 The calculation position (r) represents the radius of
 209 air cavity and z was the calculation area in
 210 millimeters. Point position of $(r \cdot \sin\theta, r \cdot \cos\theta, z)$
 211 corresponds to one voxel. Furthermore, the averaged
 212 dose cross section $\overline{D_{CS}}$ is given by Eq. (3).

$$215 \overline{D_{CS}} = \frac{1}{\pi R^2 N M} \sum_i \sum_z \sum_{r_{CS}} \sum_\theta D_p^i(r_{CS} \sin\theta, r_{CS} \cos\theta, z) \quad (3)$$

216 Here, r_{CS} is the calculated position inside the
 217 phantom in axial plane, R is the phantom radius,
 218 D_p^i is the voxel dose at the specified position in
 219 every air cavity, and M is the total number of Monte
 220 Carlo simulation. The averaged dose $\overline{D_{CS}}$ in principle
 221 is equivalent to weighted CTDI.

225 CTDI measurement

226 Direct measurement on a 3DRA machine was
 227 conducted to verify the generated coefficients from
 228 the Monte Carlo simulation. CTDI measurements
 229 were performed using the IAEA protocol on
 230 Siemens Artis Zee 3DRA fluoroscopy. A Radcal
 231 10X6-3CT ion chamber, which is 100 mm in length,
 232 was used and irradiated with two nominal tube
 233 voltage of 70 kV and 109 kV. In detail, the exposure
 234 factors in this study can be seen in Table 1.

235 Implementing the conventional weighted
 236 CTDI, CTDI_{100} was partitioned into $\text{CTDI}_{\text{center}}$ and
 237 $\text{CTDI}_{\text{periphery}}$. The dose cross section is expressed
 238 as follows in Eq. (4).

$$240 \overline{D_{CS}} = w_1(\text{CTDI}_{100})_{\text{center}} + w_2(\text{CTDI}_{100})_{\text{periphery}} \quad (4)$$

242 where w_1 and w_2 represent the CTDI_w coefficients.
 243 The solution of this linear equation was
 244 obtained using MATLAB *linsolve* library,
 245 incorporating all energy and beam width parameters.
 246 Mathematically, the *linsolve* input can be written
 247 as follows.

$$\begin{pmatrix} (CTDI_{100})^{70\text{ kV,NB}}_{center} & (CTDI_{100})^{70\text{ kV,NB}}_{periphery} \\ \vdots & \vdots \\ (CTDI_{100})^{109\text{ kV,FB}}_{center} & (CTDI_{100})^{109\text{ kV,FB}}_{periphery} \end{pmatrix} \begin{pmatrix} w_1 \\ w_2 \end{pmatrix} = \begin{pmatrix} D_{cs}^{-70\text{ kV,NB}} \\ \vdots \\ D_{cs}^{-109\text{ kV,FB}} \end{pmatrix} \quad (5)$$

249

250

251 **Table 1.** Exposure factor of each measurement on 3DRA
252 Artis Zee.
253

Parameter	20s DCT Head (70 kV)	20s DCT Head (109 kV)
Tube Voltage	70 kV	109 kV
Tube Current	236 mAs	169 mAs
Pulse Width	11.6 ms	7.3 ms
Time	20 s	20 s
Frame per second	3	3

254

255

256 **Weighted CTDI coefficients and analysis**

257 The proposed coefficient was analyzed by
258 comparing the simulated CTDI with measured
259 CTDI for the same exposure parameters, as well
260 as with conventional CTDI_w equation. By using
261 the conventional CTDI_w equation as a reference,
262 the percentage difference in CTDI_w was obtained
263 as follows.

264

$$\Delta\% = \frac{(CTDI_W^{conv} - CTDI_W^{proposed})}{CTDI_W^{conv}} \times 100\% \quad (6)$$

266

267

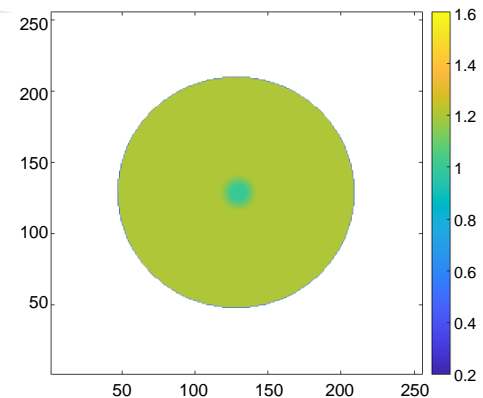
268 **RESULTS AND DISCUSSION**

269 500 million Monte Carlo particle histories
270 yield an average standard deviation of 2.99 %
271 in simulations, with a range of 1.83 % to 6.07 %.
272 To validate the Monte Carlo method, a full rotation
273 of the CBCT was simulated for all simulation
274 parameters. Before applying Eq. (5), it is necessary
275 to consider dependent factors, such as variations in
276 beam width and energy. Based on the IAEA
277 protocol regarding CBCT measurements using
278 a 100 mm detector, a comparison of the CTDI₁₀₀
279 ratio between wide and narrow beams should
280 be incorporated into the equation. In this study,
281 the comparison between Full Beam (8.6 cm) and
282 Narrow Beam (1.7 cm) yielded an average
283 ratio of 0.965 ± 0.024 for 70 kV and 0.970 ± 0.023
284 for 109 kV. This ratio indicates that the conventional
285 CTDI₁₀₀ equation can be used for measurements
286 of CBCT with a 100 mm ion chamber without
287 losing significant dose reading information.
288 This result were supported by previous research
289 conducted by Leon et al., which reported a
290 3 % difference between conventional CTDI
291 collimated beam and open beam measurements
292 [8]. Moreover, this explains that the energy
293 variation used in this study did not substantially

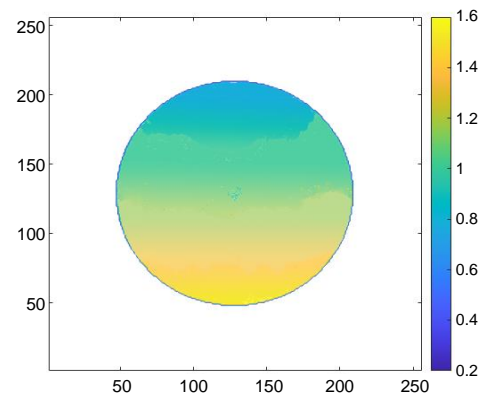
294 affect the dose-response. The Pearson correlations
295 for the energy in function of field widths of the NB,
296 WB, and FB beams showed strong correlations with
297 $r = 0.99$, $r = 0.87$, and $r = 0.98$, respectively.
298 These results are agreed with the research by
299 Markovich et al., which stated that the variation
300 in tube voltage (kV) is 2-5 % [14].

301 Figure 3a displays an axial view of
302 normalized CTDI dose distribution with air cavity at
303 the center of the phantom for one full rotation.
304 The dose distribution was evenly distributed
305 inside the phantom. Consequently, the weighting
306 ratio of CTDI_{center} and CTDI_{periphery} in this study
307 was 1:1. These results were consistent with the
308 coefficient values obtained by Kim et al.
309 for CBCT, where a 1/2 weighting factor was
310 assigned to both the middle and periphery of the
311 phantom [12]

312



(a)



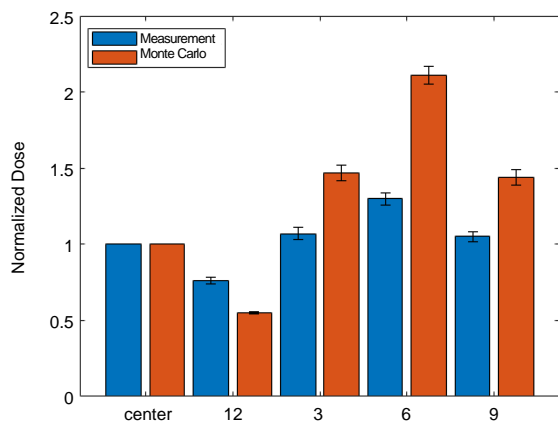
(b)

Fig 3. Typical dose distribution of CBCT Full Beam on Monte Carlo simulation with air cavity in the middle of the phantom for a) full and b) partial rotation. The partial rotation represents the 3DRA irradiation scanning of 200° rotating x-ray tube.

323 An example of the dose distribution in 3DRA 356 0.26 for the center and 0.74 for the periphery.
 324 irradiation is shown in Figure 3b. Visually, the dose 357 As a result, the proposed $CTDI_w$ equation for
 325 is notably concentrated at the bottom of the 358 evaluation on the 3DRA machine is formulated
 326 phantom, attributed to the impact of the x-ray tube 359 as follows in Eq. (7).
 327 rotation during radiation. As **CTDI weighted** is a 360
 328 relative factor, the results of Monte Carlo 361 $CTDI_w = \frac{1}{4}(CTDI_{100})_{center} + \frac{3}{4}(CTDI_{100})_{periphery}$ (7)
 329 simulations and measurements with an ionization 362
 330 chamber were normalized at the central position, as 363
 331 depicted in Table 2 and Fig. 4. There was a 364
 332 consistent trend between the simulation and ion 365
 333 chamber measurement, where the value at 12 o'clock 366
 334 being the lowest and 6 o'clock being the highest 367
 335 value. In general, Monte Carlo normalized CTDI 368
 336 values were smaller than the direct measurement. 369
 337 In contrast, at the 12 o'clock position, the simulated 370
 338 dose showed a higher value than the measurement. 371
 339 This discrepancy might be attributed to the absence 372
 340 of simulation for the patient table, which was a 373
 341 photon beam attenuator [17]. 374

342 **Table 2.** Ratio of $CTDI_{position}/CTDI_{center}$ of Monte Carlo
 343 simulation and ion chamber measurement for
 344 each energy and position.
 345
 346

Energy (keV)	Position	Monte Carlo Simulation			Ion Chamber Measurement		
		NB	WB	FB	NB	WB	FB
70	\overline{D}_{cs}	0.89	0.91	0.88			
	Center	1	1	1	1	1	1
	12 o'clock	0.78	0.78	0.72	0.55	0.55	0.54
	3 o'clock	1.06	1.11	1.1	1.46	1.41	1.39
	6 o'clock	1.31	1.4	1.37	2.09	2.11	2
109	\overline{D}_{cs}	0.84	0.86	0.91			
	Center	1	1	1	1	1	1
	12 o'clock	0.77	0.74	0.77	0.55	0.56	0.55
	3 o'clock	0.98	1.04	1.11	1.42	1.58	1.56
	6 o'clock	1.19	1.2	1.31	2.05	2.22	2.19
	9 o'clock	0.97	1.01	1.11	1.4	1.53	1.52



347 **Fig 4.** Average dose point at center, 12, 3, 6, and 9 o'clock
 348 ion chamber position for all energy and radiation width.
 349 The dose was normalized to center position of Head
 350 CTDI phantom
 351
 352
 353

354 Applying Eq. (5), the weighted CTDI 402
 355 coefficients derived in this study were found to be 403 more accurate average dose assessment for 3DRA

364 The $CTDI_w$ results for ion chamber
 365 measurements based on these proposed coefficients
 366 and the conventional equation are summarized in
 367 Table 3. Notably, the percentage differences
 368 between the proposed and conventional $CTDI_w$
 369 were within -3 %. The negative sign signifies
 370 that the $CTDI_w$ dose obtained from the proposed
 371 equation was greater than the conventional
 372 method. This observed accuracy compares favorably
 373 with the average dose interpolation method, which
 374 reported a 6 % dose difference with the $CTDI_w$
 375 conventional method for four ion chamber
 376 measurement positions on the CTDI phantom using
 377 the same machine [7].

378 **Table 3.** $CTDI_w$ different between conventional and proposed
 379 equation for 3DRA.
 380

Energy (keV)	Field Width	$CTDI_w$ (mGy)		%Δ
		conventional	proposed	
70	NB	10.39	10.64	-2.41 %
	WB	9.81	10.10	-2.96 %
	FB	7.03	7.23	-2.84 %
109	NB	10.00	10.25	-2.50 %
	WB	10.47	10.73	-2.48 %
	FB	7.05	7.20	-2.13 %

381 There were limitations to this research.
 382 Firstly, simulations and measurements were
 383 conducted only on a 3DRA machine with a
 384 200° rotation. As shown in Fig. 3, variation in the
 385 rotation during irradiation led to different dose
 386 distributions and coefficients of the $CTDI_w$.
 387 Investigating of the impact of the rotation angle of
 388 the x-ray tube on the weight coefficient is beyond
 389 the scope of this study. Secondly, this study focuses
 390 on theoretical Monte Carlo simulations and
 391 compares only with common ion chamber
 392 measurements. Further validation through
 393 experimental methods, such as using Gafchromic
 394 film could be undertaken to verify the average
 395 cross-section dose, which cannot be done using an
 396 ion chamber.
 397

400 CONCLUSION

401 In this work, Monte Carlo simulation and
 402 linear solver techniques were performed to provide a
 403 more accurate average dose assessment for 3DRA

404 irradiation. The concept of weighted CTDI was 434
 405 successfully implemented on 3DRA by replacing the 435
 406 weighting coefficients with $W_{\text{center}} = 1/4$ and 436
 407 $W_{\text{periphery}} = 3/4$. The accuracy of proposed CTDI_w 437
 408 equation differs by 3 % to conventional CTDI 438
 409 formula. These findings contribute valuable insights 439
 410 for estimating average doses using standard CTDI₁₀₀ 440
 411 protocol measurement on 3DRA. 441

412

413

414 ACKNOWLEDGMENT

415 This study was funded by Faculty of 444
 416 Mathematics and Natural Sciences Universitas 445
 417 Indonesia grant No. 019/UNF2.F3.D/PPM.00.002/2022 446
 418 447
 419

420 AUTHOR CONTRIBUTION

421 All authors read and approved the final 448
 422 version of the paper. 449
 423 450

424

425

425 REFERENCES

426 1. X. Li, J. A. Hirsch, M. M. Rehani *et al.*, Am. J. 454
 427 Roentgenol. **214** (2020) 158. 455
 428 2. W. Leitz, B. Axelsson and G. Szendrő, Radiat. 456
 429 Prot. Dosim. **57** (1995) 377. 457
 430 3. T. Berris, R. Gupta and M. M. Rehani, Am. J. 458
 431 Roentgenol. **200** (2013) 755. 459
 432 4. R. Fahrig, R. Dixon, T. Payne *et al.*, Med. Phys. 460
 433 **33** (2006) 4541. 461

462

5. Y. Kyriakou, P. Deak, O. Langner *et al.*, Phys. 434
 Med. Biol. **53** (2008) 3551. 435
 6. International Atomic Energy Agency (IAEA), 436
 IAEA Human Health Series Report 5, Status of 437
 Computed Tomography Dosimetry for Wide 438
 Cone Beam Scanners, Vienna (2011). 439
 7. E. C. Podnieks and I. S. Negus, Br. J. Radiol. 440
85 (2012) 161. 441
 8. S. Leon, J. Appl. Clin. Med. Phys. **18** 442
 (2017) 230. 443
 9. U. Lechel, C. Becker, G. Langenfeld-Jäger *et al.*, 444
 Eur. Radio. **19** (2009) 1027. 445
 10. A. Ding, Y. Gao, H. Liu *et al.*, Phys. Med. Biol. 446
60 (2015). 447
 11. C. De Mattia, F. Campanaro, F. Rottoli *et al.*, 448
 Eur. Radiol. Exp. **4** (2020) 1. 449
 12. S. Kim, H. Song, E. Samei *et al.*, J. Appl. Clin. 450
 Med. Phys. **12** (2011) 84. 451
 13. T. Haba, S. Koyama, Y. Kinomura *et al.*, Med. 452
 Phys. **44** (2017) 6603. 453
 14. A. Markovich, A. G. Morgan, F. F. Dong *et al.*, 454
 J. Med. Imaging **4** (2017) 031205. 455
 15. T. Haba, K. Yasui, Y. Saito *et al.*, Physica Med. 456
81 (2021) 130. 457
 16. J. M. Boone and J. A. Seibert, Med. Phys. **24** 458
 (1997). 459
 17. A. Abuhaimed, C. J. Martin, M. Sankaralingam, 460
et al., Phys. Med. Biol. **60** (2015) 1519. 461